The Journal of Chemical Physics

Preparation of high orbital angular momentum Rydberg states by optical-millimeter-wave STIRAP

Cite as: J. Chem. Phys. **153**, 084301 (2020); https://doi.org/10.1063/5.0017790
Submitted: 09 June 2020 . Accepted: 02 August 2020 . Published Online: 24 August 2020

T. J. Barnum, H. Herburger, D. D. Grimes, J. Jiang, and R. W. Field

The Journal of Chemical Physics ARTICLE scitation.org/journal/jcp

Preparation of high orbital angular momentum Rydberg states by optical-millimeter-wave STIRAP

Cite as: J. Chem. Phys. 153, 084301 (2020); doi: 10.1063/5.0017790
Submitted: 9 June 2020 • Accepted: 2 August 2020 •
Published Online: 24 August 2020

T. J. Barnum,[1,a] H. Herburger,[2] D. D. Grimes,[1] J. Jiang,[1,b] and R. W. Field[1,c]

AFFILIATIONS

[1] Department of Chemistry, Massachusetts Institute of Technology, Cambridge, Massachusetts 02139, USA
[2] Laboratorium für Physikalische Chemie, ETH Zürich, Vladimir-Prelog-Weg 2, 8093 Zürich, Switzerland

[a] **Electronic mail:** tbarnum@mit.edu
[b] **Present address:** Lawrence Livermore National Laboratory, 7000 East Avenue, Livermore, CA 94550, USA.
[c] **Author to whom correspondence should be addressed:** rwfield@mit.edu

ABSTRACT

Rydberg states of molecules are intrinsically challenging to study due to the presence of fast non-radiative decay pathways, such as predissociation. However, selectively exciting Rydberg states with values of the orbital angular momentum (ℓ) $\ell \gtrsim 3$ is a productive strategy to minimize this rapid decay and to populate molecular Rydberg states with lifetimes that approach those of atoms. In this proof-of-principle demonstration, we transfer population to an *nf* Rydberg state of the calcium atom by stimulated Raman adiabatic passage, in which an optical and a millimeter-wave field couple the initial and final states via an intermediate *nd* Rydberg state. Numerical simulations reproduce the observed time and frequency dependences of the population transfer and suggest the utility of this scheme to populate high-ℓ Rydberg states of molecules.

I. INTRODUCTION

Rydberg states of molecules possess many of the extreme properties, such as large polarizabilities and strong dipole–dipole interactions, that make Rydberg atoms attractive for diverse applications in quantum computation,[1] electrostatic slowing and trapping,[2,3] and high-resolution spectroscopy.[4,5] Spectroscopic investigations of molecular Rydberg states have enabled measurements of the electric structure of ions[6,7] and uncovered the complex dynamics of the exchange of energy between the molecular ion-core and the Rydberg electron.[8–10] The most significant challenge in the study of Rydberg states of molecules is the presence of fast non-radiative decay pathways. In particular, predissociation occurs due to the interaction of a bound excited state with one or more dissociation continua, which leads to dissociation of the molecule at an energy below the dissociation asymptote of the Rydberg state potential energy surface.[11] Predissociation is a universal obstacle to the systematic study of molecular Rydberg states. Through proof-of-principle experiments on atomic Rydberg states reported in this article, we propose the use of optical–millimeter-wave stimulated Raman adiabatic passage (optical–mmW STIRAP) as a general and efficient means to circumvent the predissociation obstacle that hinders the study of molecular Rydberg states.

Critical to the success of this method is the fact that, despite the ubiquity of predissociation in highly excited molecules, its impact can be reduced by excitation of carefully chosen Rydberg states. The repulsive states responsible for predissociation are valence electronic states, which invariably have a significant wavefunction amplitude localized near the ion-core. Increasing the orbital angular momentum, ℓ, of the Rydberg electron limits the interaction with repulsive valence states by reducing the amplitude of the Rydberg wavefunction near the ion-core. In a semi-classical picture, the point of the closest approach of the Rydberg electron to the ion-core in a Keplerian orbit occurs at $r_{\min} \approx \ell(\ell+1)$.[12] Thus, high-$\ell$ Rydberg states do not sample the region near the ion-core, so they interact less strongly with valence states and, therefore, are more weakly predissociated.

In general, Rydberg states with $\ell \lesssim 3$ are all core-penetrating and since the valence states also have low-ℓ character, they exhibit fast (typically, $\lesssim$1 ns) predissociation rates.[13,14] Meanwhile, states with $\ell \gtrsim 3$ are all core-nonpenetrating, and predissociation rates decrease rapidly with each step of increase in ℓ.[15]

Systematic access to high orbital angular momentum Rydberg states is restricted by the combination of the effective $\Delta\ell = \pm 1$ selection rules for dipole-allowed transitions and the short (sub-nanosecond) predissociation-limited lifetimes of low-ℓ Rydberg states. One technique that is uniquely well-suited to population transfer in the presence of short-lived intermediate states is Stimulated Raman Adiabatic Passage (STIRAP).

STIRAP has been extensively discussed in the literature and successfully applied to many systems in atomic and chemical physics.[16–19] In a three-level system, a "dark" population-trapping superposition of the initial and final states is prepared by two coherent time-varying fields. The amplitudes of these two coupling fields are changed smoothly in time to ensure adiabatic evolution of the dark state, transferring population from the field-free initial state to the final state.

In this article, we report the implementation of optical–mmW STIRAP, which relies on coherent coupling of an optical pump field and a millimeter-wave Stokes field. As a first test of this technique, we have coherently transferred $\gtrsim$50% of the total population between the 4s5p and 4s28f states of Ca atoms. Our choice of an atomic system for this initial demonstration was motivated by the ability to quantitatively characterize the time-dependent populations of all of the involved states in the absence of non-radiative decay mechanisms. We observe characteristic features of the STIRAP process in a time-delay experiment, in which enhanced population transfer occurs only in the so-called "counterintuitive" pulse timing, and a detuning experiment, in which maximal population transfer occurs whenever two-photon resonance is maintained. Numerical simulations reproduce these observations, supporting our interpretation and allowing for detailed analysis of the imperfections in our experiment. Simulation of a hypothetical predissociated (1 ns lifetime) molecular system demonstrates that, even with the current experimental shortcomings, optical–mmW STIRAP is a promising method for populating high-ℓ Rydberg states of molecules.

II. EXPERIMENT

An atomic Ca beam was generated in our ablation-loaded cryogenic buffer-gas cooled beam source. This apparatus has been described in detail previously,[20,21] and we describe only the characteristics relevant to this experiment. A schematic of the experimental apparatus appears in Fig. 1. Calcium atoms are produced by ablation of a calcium metal target by ~10 mJ pulses of the 532 nm second harmonic of a nanosecond Nd:YAG laser (Spectra Physics, GCR-130), focused to a ~1 mm^2 spot. The ablated Ca atoms thermalize in the 20 K neon buffer gas and undergo a mild hydrodynamic expansion through the output orifice of the cell. The laser and mmW radiation intersect the atomic beam transversely 30 cm downstream from the buffer-gas cell. In this interaction region, the atomic beam exhibits a transverse velocity distribution with a full width at half maximum (FWHM) of about 250 m/s. The number density of Ca

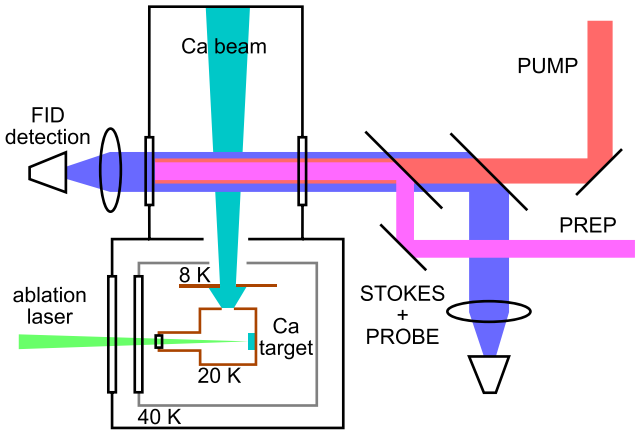

FIG. 1. Schematic of the cryogenic buffer-gas cooled beam source used in this work. Calcium atoms are laser ablated from a metal target and thermalize with neon atoms at 20 K inside the buffer-gas cell. The beam is extracted from the cell and undergoes a mild hydrodynamic expansion. Approximately, 30 cm downstream from the output of the cell, the atomic beam intersects the two laser beams and the millimeter-wave field, which all co-propagate through the chamber. Following the population transfer experiment, the populations in the intermediate 4s30d and 4s28f states are probed by polarizing two connected Rydberg–Rydberg transitions and detecting the coherent free induction decay (FID) at a second millimeter-wave horn.

atoms is estimated to be ~10^{10} cm^{-3} by laser induced fluorescence measurements.[20] Figure 2 shows the relevant Ca energy levels and radiation sources used in the experiment. The initial state in the STIRAP three-level system is populated by pumping the 4s5p ← 4s^2 transition at 272 nm with a frequency-doubled dye laser (SIRAH Cobra Stretch), referred to as the "Prep" laser hereafter. No attempt is made to characterize the absolute number of atoms in this initial state.

The pump photon couples the initial 4s5p and intermediate 4s30d states at 804 nm and is generated by pulsed amplification of a continuous wave (cw) laser. The seed laser is a commercial Ti:sapphire laser (M Squared SolsTiS) locked to a high-resolution wavemeter (Angstrom WS/7), which allows for reproducible tuning of the laser frequency during the course of an experiment. Approximately, 100 mW of cw radiation is fiber coupled to the input of a three-stage dye amplifier pumped by the second harmonic of an injection-seeded, pulsed Nd:YAG laser (Spectra Physics, LAB-170). Spatial filtering after each of the three amplification stages reduces the amplified spontaneous emission (ASE) in the output laser beam. We obtain 10 mJ, 7 ns FWHM pulses of near-infrared radiation. Details of the linewidth are discussed later in the text.

The intermediate 4s30d and final 4s28f states are coupled by a Stokes field in the mmW frequency range. This 25 ns, 263 GHz, single-frequency mmW pulse is produced by using a 260 GHz–300 GHz mmW spectrometer, which has been described in detail by the Pate group[22] and is briefly summarized here. The output of a 12.0 GS/s arbitrary waveform generator (AWG, Agilent M8150) is mixed with a phase-locked 9.375 GHz local oscillator (Miteq, DLCRO 0101-09375-3-15P) and filtered to select the higher

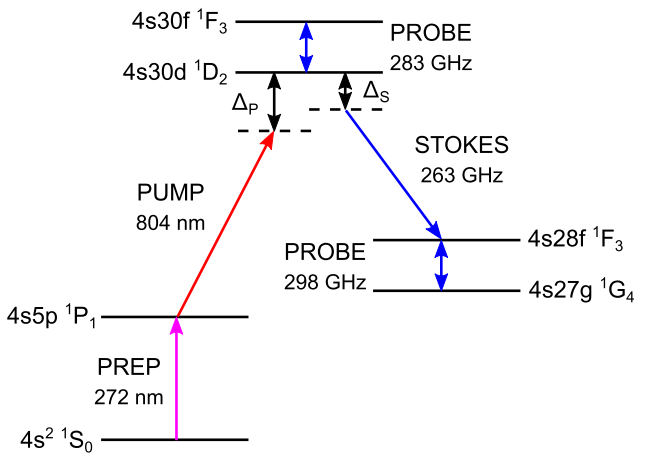

FIG. 2. Level scheme in Ca for STIRAP demonstration. The three-level system for coherent population transfer is composed of the 4s5p, 4s30d, and 4s28f singlet states, which are the initial, intermediate, and final states, respectively. The Pump laser field couples the initial and intermediate states with one-photon detuning Δ_P, and the Stokes mmW field couples the intermediate and final states with one-photon detuning Δ_S.

frequency sideband. This low-frequency waveform is sent to an active multiplier chain (AMC, Virginia Diodes AMC291), which multiplies the frequency by 24 to produce the required mmW excitation pulses. The radiation is broadcast into the chamber by a standard gain horn antenna (Millitech, SGH-10). The residual excitation pulses as well as the mmW free induction decay (FID) from the sample are received on the opposite side of the sample volume by an identical horn antenna and down-converted. The local oscillator for down-conversion is generated by a second channel of the AWG that is mixed with the same phase-locked oscillator and multiplied by a factor of 12 in a second AMC (Virginia Diodes MixAMC156). Down-conversion is accomplished in a subharmonic mixer, and the intermediate frequency signal is digitized directly on a 50 GS/s, 20 GHz digital oscilloscope (Tektronix DPO72004). The ability to create tailored sequences of mmW pulses with an AWG allows us to interrogate, on every experimental cycle, the populations of the intermediate and final states of our three-level system by two linked "Probe" transitions. Note that all pulses from the mmW spectrometer are constrained by technical limitations to have square temporal profiles with rise and fall times of less than 2 ns. This non-ideal pulse shape is explicitly included in the numerical simulations and profoundly influences the quality of the population transfer.

The population transfer efficiency and the capability for numerical characterization of our STIRAP scheme require a sample volume in which each of the multiple radiation fields has a well-known spatial profile. The sample volume is defined by the Prep and Pump laser fields, which are collimated to $1/e^2$ beam diameters of ~7 mm and 10 mm, respectively, while the mmW radiation is approximately collimated by using a Teflon lens to a cross sectional area of 10 cm^2. The mmW radiation is first overlapped with the 804 nm laser beam at an ITO-coated glass plate, which acts as a mirror at mmW frequencies. These two radiation fields are then overlapped with the 272 nm Prep laser beam by transmission through a large-diameter backside-polished mirror coated for reflectivity near 266 nm (CVI, Y4-3037-45-UNP).

The coherent couplings of the initial to intermediate states and the intermediate to final states are characterized by the Rabi frequencies of the Pump and Stokes pulses, Ω_P and Ω_S. The Rabi frequency is defined as

$$\Omega(t) = \frac{\vec{\mu} \cdot \vec{E}(t)}{\hbar}, \tag{1}$$

where $\vec{\mu}$ is the transition dipole moment and $\vec{E}(t)$ is the time-dependent electric field envelope of the relevant pulse of radiation. In addition, the STIRAP process is parameterized in terms of detuning of the Pump and Stokes fields from one-photon resonance, Δ_P and Δ_S. The detunings are illustrated in Fig. 2 and defined as the difference between the transition frequency and the carrier frequency of the Stokes or the Pump field,

$$\hbar\Delta_P = E_2 - E_1 - \hbar\omega_P, \tag{2}$$

$$\hbar\Delta_S = E_2 - E_3 - \hbar\omega_S, \tag{3}$$

where E_1, E_2, and E_3 are the energies of the initial, intermediate, and final states, respectively, and ω_P and ω_S are the angular frequencies of the Pump and Stokes fields. The population transfer efficiency of STIRAP is especially insensitive to the one-photon detuning of the system, $\Delta = (\Delta_P + \Delta_S)/2$, but is strongly modified by the two-photon detuning $\delta = (\Delta_P - \Delta_S)$.

A. Frequency chirp measurement

A well-known problem associated with pulsed amplification in a dye solution is frequency chirping in the amplified laser pulse.[23,24] We characterize this phenomenon, as in previous studies, by a self-heterodyne measurement. A portion of the seed laser is frequency-shifted by double-passing an acousto-optic modulator (Gooch and Housego, AOMO 3350-125) operating at 375 MHz. This frequency-shifted radiation, along with the output of the pulsed amplification chain, is coupled into a single-mode fiber to overlap the wavefronts of the two laser beams. The beat note between the two lasers is monitored on a fast photodiode (Newport, 818-BB-21A) and digitized on a high-speed oscilloscope (Tektronix, DPO71254B). By using a large frequency offset of 750 MHz, we can fit the resultant beat pattern directly in the time domain and extract the time-dependent frequency chirp. We typically observe a chirp of ~50 MHz between the initial and final 10% intensity limits of the pulse, which causes the pulsed output to be broadened beyond the Fourier transform limit. This effect is explicitly included in our numerical simulations as a time-dependent one-photon detuning.

B. Doppler broadening

The Doppler broadening present in the atomic sample is a key parameter in the STIRAP experiment. A Doppler shift of the relevant transitions can create a two-photon detuning, which would significantly reduce the population transfer efficiency. The geometry of the experiment can be chosen to reduce this effect. If the Pump and Stokes radiation fields have similar frequencies, the Doppler shift

will be similar for each velocity sub-group. For a Λ arrangement of energy levels, the Pump and Stokes pulses should co-propagate across the sample, while for a ladder arrangement, the two pulses should counter-propagate. The nearly equal Doppler shifts produce only a one-photon detuning, while maintaining the all-important two-photon resonance. Unfortunately, as the frequency difference between the two photons increases, the cancellation of the Doppler shifts is reduced. In the case of optical–mmW STIRAP, the optical and mmW photons differ in frequency by approximately three orders of magnitude, and as a result, there is negligible cancellation of the Doppler shifts for the two photons. Therefore, the Doppler shift of the Pump photon across the sample produces a range of two-photon detunings across the sample. In this experiment, a cryogenic buffer-gas beam, with its typically small divergence ($\theta_{\mathrm{FWHM}} \approx 65^{\circ}$), reduces the transverse Doppler broadening, while also allowing for the large interaction volume necessary for FID-detected mmW spectroscopy experiments on Rydberg states.[25] The observed 310 MHz linewidth for the Pump 4s30d ← 4s5p transition at 804 nm corresponds to a transverse velocity spread of 249 m/s FWHM. This velocity spread produces a Doppler width of ~219 kHz for the Stokes transition at 263 GHz. For simulations of the STIRAP experiment, we neglect this <0.1% cancellation between the 310 MHz and 215 kHz Doppler widths.

C. Population calibration

In order to quantify the population distribution among the three STIRAP-involved levels, we developed a calibration experiment, which employs a sequential, adiabatic rapid passage (ARP) excitation scheme. A schematic timing diagram of the experimental sequences for the calibration procedure and the time-delay experiment appear in Fig. 3. In the time-delay experiment, the delay time between the 263 GHz Stokes pulse and the 804 nm Pump pulse is scanned in 1 ns time steps. At each choice of the time delay, the population remaining in the intermediate and final states is measured by polarizing the two Probe transitions with single-frequency mmW pulses and detecting the subsequent Rydberg–Rydberg FID signal. For the calibration experiment, we have observed saturation of the 4s30d ← 4s5p transition as a function of Pump laser power. As a result of the large number of Rabi oscillations induced by the laser pulse and moderate pulse-to-pulse energy fluctuations, we measure an average 50% population transfer between the two levels. Following laser excitation, we apply an mmW field with a 300 ns cubic frequency chirp ($f_{\mathrm{inst}} \propto t^3$) of 800 MHz centered at the Stokes transition frequency. This produces a complete population transfer (≳95%) to the final state. Probe pulses of identical power and duration are used in the calibration and STIRAP time-delay experiments, allowing direct comparison of the signal from the intermediate to final state transitions. We switch between the calibration and time-delay sequences after every choice of time delay for the STIRAP experiment. Thus, we have a 50% total population transfer signal with which we calibrate the STIRAP transfer. This calibration scheme additionally corrects for the slow fluctuations in the total signal due to the ablation source and the Prep laser.

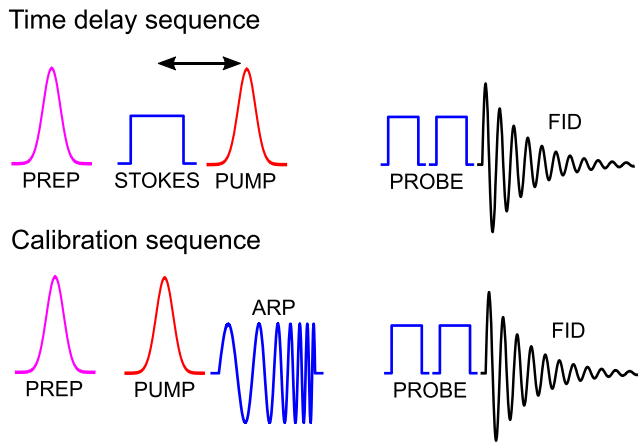

FIG. 3. Schematic timing diagram for the time-delay and calibration experiments as described in the text. In the time-delay sequence, the Prep pulse arrives well before the Stokes and Pump pulses, and the time delay between Stokes and Pump pulses is scanned. In the calibration sequence, the Prep and Pump pulses are followed by an mmW frequency chirp that induces an adiabatic rapid passage (ARP) to transfer all population from the intermediate to final states. Each timing sequence concludes with the polarization of the two probe transitions, followed by FID detection to measure both the intermediate and final state populations.

D. Numerical simulations

We have simulated the population transfer in this experiment by numerical integration of the Liouville–von Neumann equation using properties for the atomic ensemble and the two photons consistent with the experiment,

$$i\hbar\frac{\mathrm{d}\rho}{\mathrm{d}t} = [H,\rho] + \Gamma, \tag{4}$$

where ρ is the density matrix for the three-level system and H is the total Hamiltonian for the atom-radiation system, which is given by

$$H = \frac{\hbar}{2}\begin{pmatrix} 0 & \Omega_{\mathrm{P}}(t) & 0 \\ \Omega_{\mathrm{P}}(t) & 2\Delta_{\mathrm{P}} & \Omega_{\mathrm{S}}(t) \\ 0 & \Omega_{\mathrm{S}}(t) & 2(\Delta_{\mathrm{P}} - \Delta_{\mathrm{S}}) \end{pmatrix}. \tag{5}$$

In Eq. (4), the operator Γ is a phenomenological decay matrix, which, considering only the predissociation of the intermediate level, has the form

$$\Gamma = \begin{pmatrix} 0 & -\frac{\gamma}{2}\rho_{12} & 0 \\ -\frac{\gamma}{2}\rho_{21} & -\gamma\rho_{22} & -\frac{\gamma}{2}\rho_{23} \\ 0 & \frac{-\gamma}{2}\rho_{32} & 0 \end{pmatrix}, \tag{6}$$

where γ is the predissociation rate of the intermediate state (State 2). By substituting the explicit forms of the total Hamiltonian [Eq. (5)] and the decay operator [Eq. (6)] into Eq. (4), we obtain a system of nine coupled differential equations, which completely describe the time evolution of the populations and coherences of the system of interest.

In our simulations, we find that the relevant Rabi frequencies, $\Omega_{\mathrm{P}} = 2\pi \times 115$ MHz and $\Omega_{\mathrm{S}} = 2\pi \times 68$ MHz, best reproduce the experimental observations. The population transfer is integrated

over the observed 310 MHz FWHM Doppler width of the Pump laser transition and the Gaussian variation of the Pump laser intensity across the laser beam profile. Both Gaussian-distributed fluctuations of the Pump laser intensity and fluctuations in the magnitude of the Pump laser chirp are explicitly included. We average 100 simulations in order to compare the simulated time and frequency dependences with the experimental results.

III. RESULTS AND DISCUSSION

A. Adiabaticity

We begin by noting that the Rabi frequencies used in our simulation should be considered *effective* Rabi frequencies. While several of the experimental imperfections have been explicitly modeled in the simulations, all neglected imperfections will have the general effect of reducing the Rabi frequencies that describe the experiment. Based on our measurement of the pulse energies and durations, both the Stokes and Pump Rabi frequencies used in the simulations are about 40% smaller than our initial estimates. Simulations that use the initially estimated Rabi frequencies show significantly worse agreement with all experimental data. In the following sections of this discussion, we will address in detail the experimental imperfections that could give rise to some of the discrepancies between the simulations and the experiment.

The STIRAP process requires adiabatic evolution of the dark state in order to coherently transfer population from the initial to the final state. Bergmann and co-workers suggested a global adiabaticity requirement for the STIRAP process,[16]

$$\Omega_{\text{eff}}\Delta\tau > 10, \tag{7}$$

where $\Delta\tau$ is the time period during which the pulses overlap and $\Omega_{\text{eff}} = \sqrt{\Omega_P^2 + \Omega_S^2}$ is the effective Rabi frequency of the system. The global adiabaticity requirement in Eq. (7) provides an approximate benchmark for determining the effectiveness of STIRAP. Our effective Rabi frequencies and pulse overlap time result in $\Omega_{\text{eff}}\Delta\tau \approx 5$. While the detailed pulse shape and other parameters will impact the final population transfer, this simple $\Omega_{\text{eff}}\Delta\tau$ metric indicates that our experiment is operating near to but not deeply in the adiabatic regime. This fact is primarily responsible for the less than perfect, ~50%, population transfer to the final state.

The second major impediment to adiabatic following in our experiment is the nearly square temporal profile of the mmW pulse. The sharp turn-on and turn-off of the Stokes pulse are antithetical to the required slow, smoothly change in Rabi frequencies, and locally violate the adiabaticity requirement. As a result, the peak population transfer occurs at a smaller negative pulse delay than that might be expected from the naive picture typically discussed, where the optimum pulse delay for two identical, smooth Gaussian pulses is equal to the pulse duration.[16,26] In our experiment, the poor adiabatic following due to the square pulse shape is partly compensated by a longer overlap time. This appears in both the experimental data and the simulation results discussed in Sec. III B. In the simulation, arbitrarily increasing the Rabi frequencies causes the optimal pulse delay timing to shift to longer negative pulse delays as the adiabatic following improves.

B. Time dependence

A typical time-delay experiment involves scanning the time delay between the Pump pulse and the Stokes pulse, while monitoring the populations of the intermediate and final levels. A schematic representation of the Pump and Stokes pulse timing is shown above the main plot in Fig. 4. For all time dependence experiments, the one-photon detunings of the Pump and Stokes pulses are set to zero. At a large negative delay, the laser pulse arrives well after the mmW pulse, and thus, only the intermediate level is populated. At a large positive delay, the laser pulse arrives well before the mmW pulse and corresponds to the regime of sequential excitation of the three-level system. Between these limits, we anticipate enhanced population transfer to the final level at short negative delays, when the pulses are in the "counterintuitive" timing, which is a key requirement of the STIRAP process.

The results of a time-delay experiment are shown as red (intermediate state) and blue (final state) markers in Fig. 4. At a short negative delay, we observe an enhanced population transfer to the final state of $\gtrsim$50%. Concurrently, the population in the intermediate state exhibits a pronounced dip. As the delay becomes positive while the two pulses are still overlapped, the population transfers to both the final and intermediate levels show variations with pulse delay that is enhanced relative to the sequential excitation regime. The intermediate state population reaches a maximum, and the final state population dips at zero time delay.

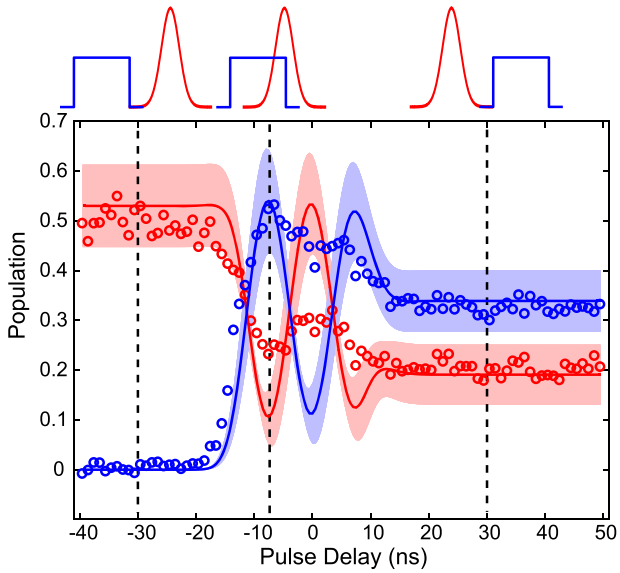

FIG. 4. Population measured in the intermediate (red markers) and final (blue markers) states as a function of delay time between the Pump and Stokes pulses. At short negative delay times, enhanced population transfer to the final state is evident, while a dip in the population of the intermediate state occurs simultaneously. A schematic representation of the Pump (red, Gaussian) and Stokes (blue, square) pulse timings appears above the main figure. The results of our numerical simulations also appear in the figure for the intermediate (red) and final (blue) states. For 100 simulations, the solid lines represent the mean population in each state, and the shaded area represents the standard deviation of the 100 simulation results.

After this point, the final state population increases slightly as the intermediate state population begins to decrease. This type of population transfer has been observed in other systems,[17,27,28] and we interpret this as further evidence for strong two-photon coupling.

Our simulations qualitatively capture many of the features of the time-delay experiment. In Fig. 4, the solid lines are the average of 100 simulations, and the shaded area represents the standard deviation of the 100 simulations. Red denotes the intermediate state, and blue denotes the final state. Population transfer of at least 50% is observed in both experimental and simulation results. This enhanced population transfer to the final state is, as expected, accompanied by a pronounced decrease in the population transfer to the intermediate state. While the calculation yields quantitative agreement with the final state population, the observed intermediate state population is about 10% larger than that in the calculation. As the pulse delay increases beyond the STIRAP timing, while the two pulses overlap, the simulation produces oscillations in the final and intermediate state populations. This oscillatory behavior is due to two-photon Rabi flopping between the initial and final levels. While we observe some time dependence of the final and intermediate state populations in the experimental data, the oscillations are strongly damped relative to the simulation.

The population transfer at long delay times is quantitatively reproduced. At long negative delays, the simulation captures the ~50% population transfer expected from our measurement of saturation of the 4s30d ← 4s5p transition. At long positive delays, the Pump and Stokes pulses interact with the system sequentially, and the final and intermediate state populations are simply dependent on the ratio of Stokes and Pump Rabi frequencies.

We hypothesize that the reduced contrast in the Rabi flopping during the pulse overlap is a result of imperfections in either the laser or mmW fields, which have not been accounted for in our simulation. These include variations or fluctuations in amplitude and polarization. Amplitude variations can take the form of hot spots in the beam profile, which can enhance the local electric field by more than 50%,[29] or uneven illumination, which is particularly difficult to characterize for the mmW field. Polarization also plays an important role that we have not yet addressed. In these experiments, all three radiation fields nominally have linear, parallel polarization. Unintentional changes to the polarization arrangement will introduce additional magnetic (m) sub-levels of the $(2\ell + 1)$-fold degenerate manifold for each state. The transition dipole moment is m-dependent, so the presence of more than one magnetic sub-level and more than one transition path produces several sets of alternate three-level systems, each with a different effective Rabi frequency. Moreover, these additional excitation paths can result in both constructive and destructive interference, as discussed by previous authors.[17,30]

We have simulated several hypothetical scenarios, including larger laser power fluctuations, non-uniform spatial profiles, and alternate polarization (more than one m sub-level) arrangements. The peak population transfer at the STIRAP timing is essentially unchanged in the presence of these additional imperfections because the STIRAP process is robust with respect to variations in the Rabi frequencies as long as the Rabi frequencies are large enough to ensure adiabatic following. In contrast, the two-photon Rabi oscillations that follow the STIRAP timing are substantially damped by these imperfections since Rabi flopping is highly sensitive to the Rabi frequency. We have been unable to characterize the laser and mmW fields in sufficient detail to unambiguously identify which of these experimental imperfections, or what combination, is dominantly responsible for the damped Rabi flopping observed.

C. Frequency dependence

The other signature of STIRAP-mediated population transfer is its insensitivity to one-photon detuning, as long as the two-photon resonance is maintained. This characteristic, which arises from the two-photon nature of the population transfer, produces a "STIRAP ridge" of enhanced population transfer at zero two-photon detuning as the Pump and Stokes detunings are varied.

Figure 5(a) and 5(b) show the final state population transfer at the STIRAP timing as a function of Pump laser detuning for several fixed values of the Stokes microwave frequency. The spectra are obtained by scanning the Pump detuning while maintaining the Stokes detuning at a fixed value. Figure 5(b) shows positive detunings from 600 MHz (dark blue) to 0 MHz (dark red) in steps of 50 MHz, and Fig. 5(a) shows negative Stokes detunings from −600 MHz (dark blue) to 0 MHz (dark red) in 50 MHz steps. All spectra were scaled by the population transfer measured at the STIRAP timing in the time-delay experiment.

The solid line for each spectrum in Fig. 5 is a fit to the data with a skew Gaussian function of the form

$$f(\nu) = A\left[1 + \mathrm{erf}\left(\frac{\alpha(\nu-\mu)}{\sigma\sqrt{2}}\right)\right]\exp\left(-(\nu-\mu)^2/2\sigma^2\right), \qquad (8)$$

where A is the scaling factor, μ is the center of the distribution, σ^2 is the variance, and α is the skewness parameter. This choice of line shape is not motivated by the physics of the system, but rather, it has a simple functional form that can capture the asymmetry, width, and shift of the observed lines. In fact, the physics that produces the observed population transfer profiles includes many contributions, and the line shape likely does not have a simple analytical form for the particular experiment described here.[31,32]

In Figs. 5(a) and 5(b), the Pump detuning that produces peak population transfer shifts as a function of the Stokes detuning. The Pump detuning of the peak population transfer approaches 400 MHz for a Stokes detuning of 600 MHz and approaches −400 MHz for a Stokes detuning of −600 MHz. The peak population transfer along this line of approximately zero two-photon detunings is the characteristic STIRAP ridge. The linewidth for all detuning values is substantially larger than the 310 MHz Doppler width due to the Pump laser. Finally, as the Stokes detuning is increased, the shape of the line becomes increasingly asymmetric, with its tail pointing toward zero Pump detuning.

The simulation of the frequency detuning experiment, shown in Figs. 5(c) and 5(d), captures many of the features observed in our experiment. In both experiment and simulation, as the Stokes detuning is increased, the Pump detuning spectra show a clear

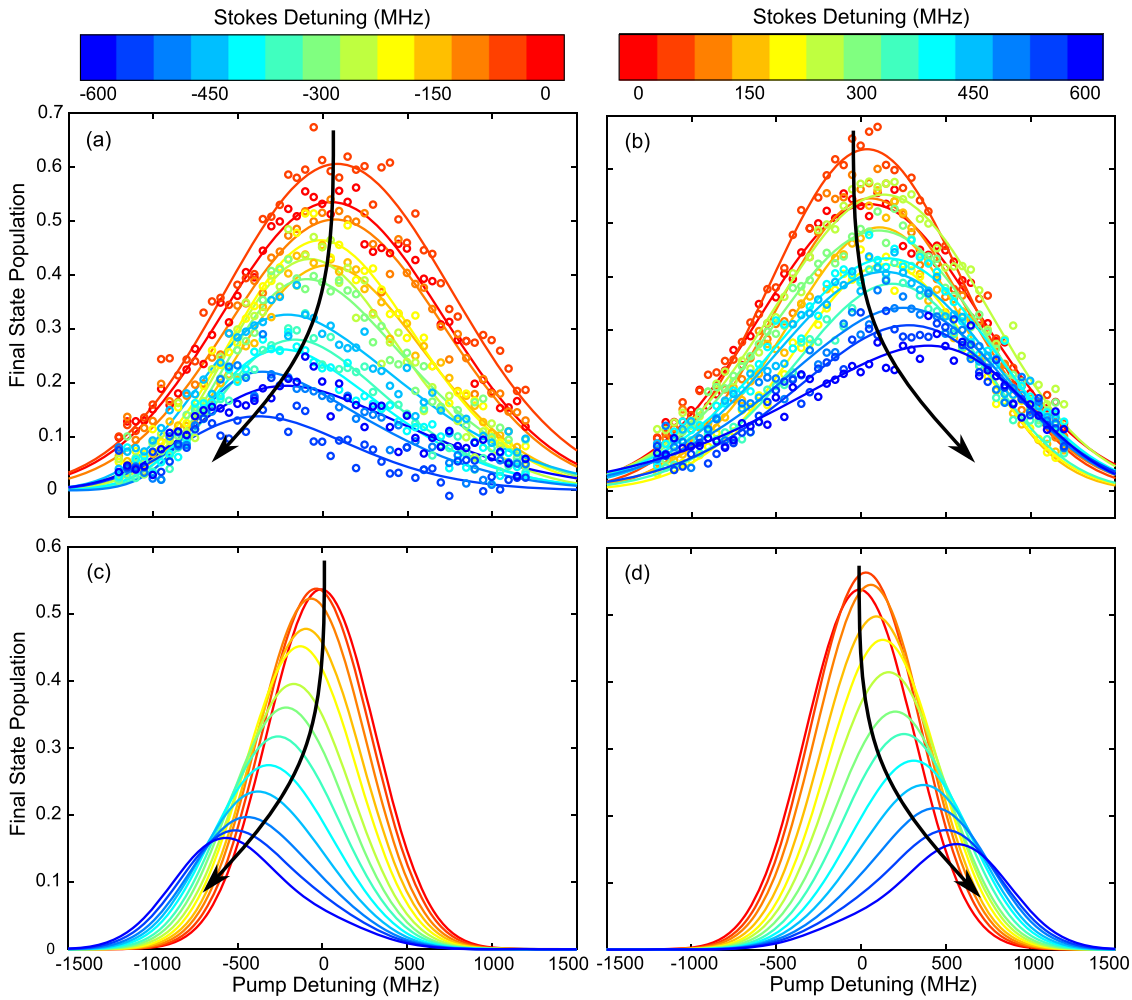

FIG. 5. Population transfer to the final state as a function of laser (Pump) detuning for fixed millimeter-wave (Stokes) detunings. (a) Stokes detunings from −600 MHz (dark blue) to 0 MHz (dark red) in steps of 50 MHz. (b) Stokes detunings from +600 MHz (dark blue) to 0 MHz (dark red). The solid lines are fits to the data with a skew Gaussian function as defined in the text. The "STIRAP ridge" (shown as a curved black arrow) is the peak population transfer that occurs along the approximate zero two-photon detuning line. (c) and (d) are the simulation results for the population transfer as functions of Pump detuning for fixed values of the Stokes detuning. (c) and (d) show Stokes detunings and color schemes identical to those of (a) and (b), respectively. Again, the black arrow is a guide to the eye, highlighting the STIRAP ridge of peak population transfer.

frequency shift in the peak population transfer along with a pronounced increase in line shape asymmetry. In order to make a more quantitative comparison, Fig. 6 shows the maximum of the fits to the experimental data (red circles) and the maximum of the simulated population transfer (black circles) as a function of Stokes detuning. The black dashed line is the naive expectation for a STIRAP process in which the peak population transfer occurs at exactly $\Delta_P = \Delta_S$. Both the experiment and simulation deviate from this naive expectation, and the rate of change of the peak transfer detuning is much shallower near one-photon resonance. As the detuning increases, the rate of change of the peak Pump detuning increases, and the value of the peak Pump detuning approaches the two-photon resonance line. The experimental results show a similar trend in the detuning dependence, although the magnitude of the observed shift, particularly at large Stokes detunings, is smaller than that expected from the simulations.

Next, we turn to an examination of the line shape. The simulation shows that in the STIRAP timing, the linewidth of the two-photon process is broader than the one-photon Doppler linewidth of 310 MHz, which is explicitly included in the simulation. The large Rabi frequencies in the STIRAP experiment allow for enhanced population transfer even in the presence of a one-photon detuning. The experimental broadening is even larger than the simulated broadening. As mentioned in Sec. III A, the effective Rabi frequencies in our simulations are smaller than those expected for the measured pulse energies and durations of the Pump and Stokes pulses. This

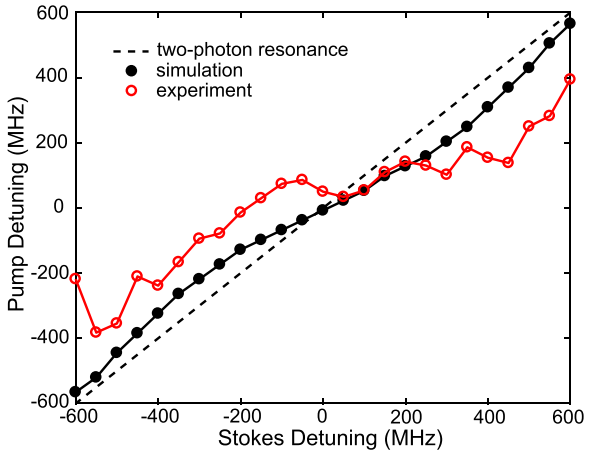

FIG. 6. The Pump detuning that produces the peak population transfer as a function of Stokes detuning. The experimental data are shown as red circles, and the simulated data as black circles. The dashed black line is the two-photon resonance line, $\Delta_P = \Delta_S$. Both the experiment and simulation exhibit deviation from the two-photon resonance line above and below one-photon resonance.

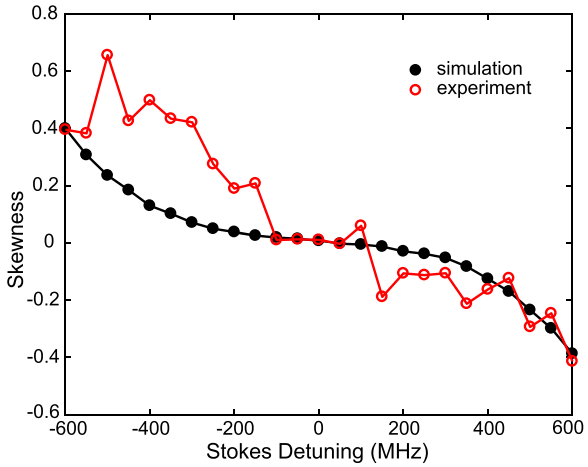

FIG. 7. Skewness ($\tilde{\mu}_3$) of the observed (red) and simulated (black) line shapes for each value of the Stokes detuning. As the Stokes detuning is increased, the asymmetry of the line shape increases due to non-adiabatic population transfer when the Pump field is tuned to one-photon resonance.

suggests that fluctuations in phase or amplitude degrade the overall coherence. These imperfections can increase the observed linewidth by broadening the laser or mmW bandwidth, or by increasing the effect of power broadening.[33]

Both the simulation and the experiment show line shapes that grow increasingly asymmetric as the one-photon detuning is increased. This is in contrast to the symmetric line shapes obtained from the simulation of a "perfect" STIRAP experiment. We quantitatively compare this asymmetry by examining the skewness of the fitted and simulated lines. Skewness is defined as the third standardized moment, given by the expression

$$\tilde{\mu}_3 = \frac{\mu_3}{\sigma^3} = \frac{E\left[(X-\mu)^3\right]}{(E\left[(X-\mu)^2\right])^{3/2}}, \tag{9}$$

where μ_3 is the third moment about the mean defined by the expectation value ($E[\cdot]$) of the quantity $(X-\mu)^3$, where X is the sample and μ is the sample mean. The standard deviation, σ, is defined in the usual way as the square root of the second moment about the mean, $(E\left[(X-\mu)^2\right])^{1/2}$. For comparison, a Gaussian distribution is symmetric and has a skewness of zero. The skewness values of the simulated (black) and fitted (red) lines are shown in Fig. 7. The calculated skewness quantitatively agrees for small negative and all positive Stokes detuned spectra. There is a greater deviation for the negative Stokes detuned spectra, though the direction and order of magnitude are correct. We interpret the similar line shapes between the simulation and experiment to mean that our simulation likely captures most of the physics, though estimates for the particular parameters (e.g., Rabi frequencies, frequency or amplitude fluctuations, etc.) may not be exactly correct.

We hypothesize that the reason for the observed asymmetry in the population transfer is the presence of non-adiabatic transitions from the initial to the final state caused by the frequency fluctuations in the Pump field and the sharp turn-off of the Stokes field. As a result, there is greater population transfer when the Pump frequency is tuned to one-photon resonance. This effect is enhanced by the presence of Doppler broadening in our sample because a Doppler sub-group with a significant population is one-photon resonant with the Pump transition even at detunings of several hundred megahertz. By varying values of the temporal pulse overlap and detuning in the simulation, we have observed simulated spectra that are double-peaked, with a second local maximum in the population transfer near zero Pump detuning. This further suggests that the population transfer in the tail is due to non-adiabatic transitions or, in other words, stepwise transitions from the initial to intermediate to final states caused mainly by the sharp turn-on of the mmW pulse. These stepwise, non-adiabatic transitions are more sensitive to one-photon detuning than STIRAP. Furthermore, we observe in the simulations that when the Stokes detuning is increased beyond the ±600 MHz region investigated experimentally, the intensity in the tail rapidly decreases, and eventually, the line shape becomes symmetric again when only the adiabatic process contributes.

We have so far considered that the result of non-adiabatic transitions is to cause greater population transfer to the final state. However, if the excitation is partly incoherent or substantially modified by pulse-to-pulse intensity fluctuations, then saturation occurs, limiting the population transfer to maximally 50%. The STIRAP process has no such limitation and can transfer up to 100% of the population from the inital to final states. This means that it is possible for non-adiabatic transitions to actually reduce the total population transfer by moving population from the final state back to the intermediate state. In both the experimental data and simulations presented in Fig. 5, there is a small dip in the population transfer when both Pump and Stokes fields are on one-photon resonance; the dark red curve has a lower maximum than the orange curves on either side. At small detunings above and below one-photon resonance, we observe slightly enhanced population

transfer to the final state. This is expected behavior because the maximum adiabatic and non-adiabatic population transfers occur near one-photon resonance, but the adiabatic transfer efficiency is much less sensitive to one-photon detuning. The non-adiabatic population transfer reduces the population transfer that would be expected for the adiabatic process alone. In both experimental and simulation results, the difference in population transfer at small detunings is subtle and merits further investigation. However, previous STIRAP experiments have reported this effect, especially when a fast intermediate state decay is involved, because non-adiabatic transitions to the intermediate state lead to irreversible loss of that population.[28]

D. Lossy intermediate state

It is informative to examine how our system behaves in the presence of a hypothetical lossy intermediate state. All simulation parameters are the same as those previously described, but the intermediate state is assumed to have a 1 ns non-radiative lifetime. This is a typical predissociation lifetime for a low-ℓ Rydberg state in a diatomic molecule.[13,14,34] Figure 8 shows the population transfer to the intermediate (red) and final (blue) states as a function of pulse delay. In the presence of this rapid decay channel, significant population transfer to the final state only occurs at the STIRAP timing. At all other times, either through sequential excitation or two-photon Rabi flopping, population is moved to the intermediate state and immediately lost. The very modest population transfer of just over 10% is a reflection of the previously described experimental imperfections in our system.

Figure 9 shows the simulated population transfer as a function of detuning with a 1 ns intermediate state lifetime. As observed in the time-delay simulation in Fig. 8, the peak transfer on resonance is just larger than 10% of that for this hypothetical system.

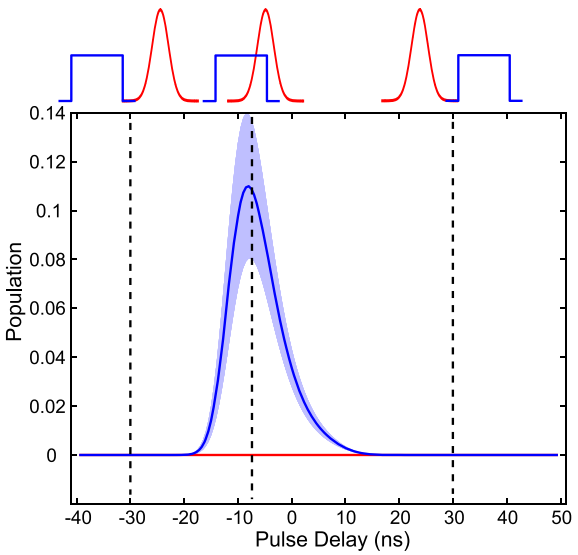

FIG. 8. Simulation results for the intermediate (red) and final (blue) state population transfers as functions of pulse delay when the intermediate state has a non-radiative lifetime of 1 ns. The solid lines are the mean population, and the standard deviation of the 100 simulations is shown as a shaded area. A schematic representation of the Pump (red, Gaussian) and Stokes (blue, square) pulse timing appears above the main figure.

As the one-photon detuning is increased, the population transfer appears more robust than that in the case with no intermediate state decay. At the extreme detunings, the population transfer decreases to ~70% of its maximal value. In contrast, the population transfer in the case with no decay (Fig. 5) is just 28% of its maximal value at the extreme detunings. In addition, the lines are significantly more symmetric, missing the long tails in the direction of zero Pump detuning. Both of these observations point to the fact that only adiabatic population transfer can move significant population from the initial to the final state in the presence of a very lossy intermediate state. Since non-adiabatic population transfer near zero Pump detuning is not effective in moving population to the final state, the line shape is more symmetric and the magnitude of the population transfer is similar for all detunings. STIRAP is characteristically insensitive to the one-photon detuning, so the adiabatic population transfer does not decrease substantially across the detuning range. In contrast, for the case with no decay, the non-adiabatic population transfer is strongly one-photon dependent and displays a dramatic increase in the population transfer only near zero Pump detuning.

This hypothetical lossy state is the true test of STIRAP. A defining feature of STIRAP is that the intermediate state is not substantially populated en route to the final state. By simulating a fast intermediate state decay, the sequential excitation path is turned off, and only STIRAP transfer can produce a signal. In our previous work, this test was the clear indication that STIRAP had *not* been achieved.[27] These simulation results imply that at least 10% of the total population is trapped in the coherent dark state in our experiment. This positive result further bolsters our interpretation that optical–mmW STIRAP is operative, though not ideal, in our experiment, and that implementation of this technique in a molecule under similar conditions would be feasible.

E. Future improvements

The final state population transfer of just over 50% for this proof-of-principle system is far below the near-unity population transfer typically associated with STIRAP. Beyond simply increasing the Rabi frequencies or eliminating the possible experimental imperfections discussed in Sec. III B, our simulations suggest the most important areas for improvement in the experimental design.

First, the mmW pulse with a nearly square temporal profile immediately hinders the adiabatic following necessary for STIRAP. The sharp turn-on and turn-off produce non-adiabatic transitions between the intermediate and final states, corrupting the purity of the desired dark state. In the mmW frequency range, arbitrary pulse shaping on nanosecond time scales is currently technically inaccessible. We have explored strategies for some pulse shaping using electrically tuned variable attenuators or up-conversion of low-frequency shaped pulses in harmonic mixers.[27] We anticipate that this challenge will be solved by the rapid advances in diode technology in this high frequency range.

The Pump laser has a near-Gaussian transverse beam profile; as a result, the Rabi frequency varies significantly as a function

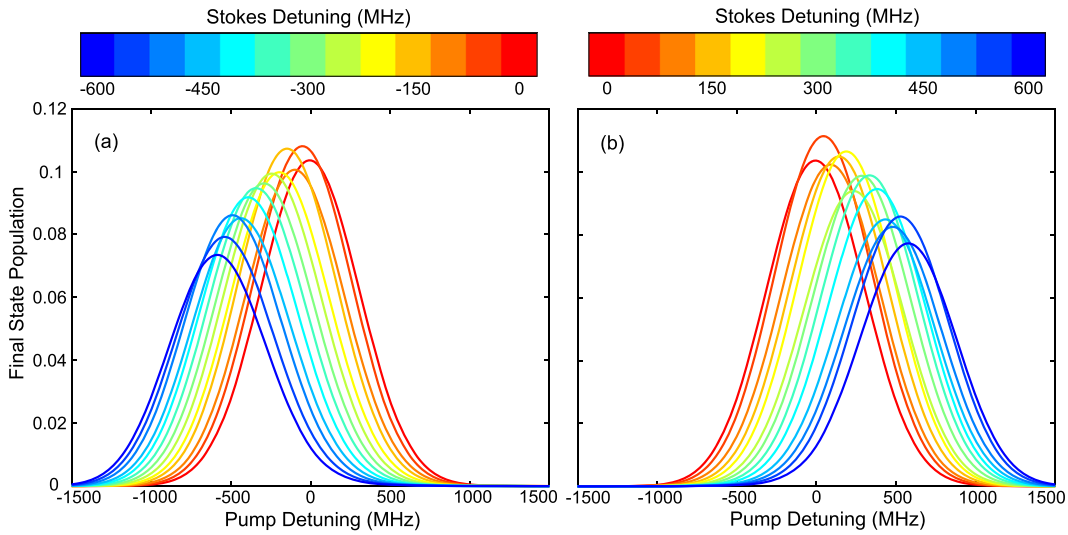

FIG. 9. Simulation results for the population transfer as functions of Pump detuning for fixed values of the Stokes detuning for a system with a 1 ns intermediate state lifetime. (a) Stokes detunings of −600 MHz (dark blue) to 0 MHz (dark red) in steps of 50 MHz. (b) Stokes detunings of 600 MHz (dark blue) to 0 MHz (dark red) in steps of −50 MHz.

of the radial dimension of the laser spot. Near the center of the Pump beam, where the laser intensity is greatest, the simulated transfer plateaus around 65% and the intermediate state population is only 20%. Moving out toward the edge of the beam profile, the population transfer efficiency decreases precipitously because the Rabi frequency is too low to ensure adiabatic following. This issue of radial variation in laser intensity has been identified in other STIRAP experiments.[35] By re-shaping the beam, for instance to a top-hat profile, it should be possible to achieve uniform population transfer efficiency across the full diameter of the laser beam.

We have simulated our experiment with corrections for these two deficiencies: both Pump and Stokes fields have a 7 ns Gaussian time profile with a peak Rabi frequency, $\Omega = 2\pi \times 150$ MHz, and both fields have top-hat profiles, with no radial variation in Rabi frequency. This new simulation predicts just over 70% population transfer from the initial to the final state. We anticipate that future implementations of optical–mmW STIRAP will correct these experimental imperfections and obtain population transfer similar to this simulation.

One of the most significant challenges in optical–mmW STIRAP relative to previous STIRAP implementations is the very large frequency difference that leads to negligible cancellation in Doppler shifts for the two photons. The use of a buffer-gas cooled beam, with its relatively low beam divergence, certainly improved the population transfer efficiency in this experiment relative to what would be possible with a high divergence supersonic jet. For reference, the Doppler width at 804 nm for a Ne supersonic jet is ~1.6 GHz, five times the value in our buffer-gas beam. By skimming the beam, the transverse Doppler width could be further reduced, although at the expense of the total number of atoms/molecules. Of interest to experiments in the ultracold regime, negligible Doppler broadening can provide a significant boost in population transfer. For the simulation of the improved experiment described in the previous paragraph, neglecting Doppler broadening eliminates the two-photon detuning in the sample and further improves the population transfer to nearly 80%.

IV. CONCLUSION

We have demonstrated population of high-ℓ Rydberg states by optical–mmW STIRAP. Population transfer occurs from a low-lying excited state of Ca atoms to an nf Rydberg state via an optically accessible lower-ℓ Rydberg state and involves coherent coupling of a laser and a mmW photon, which differ by three orders of magnitude in frequency. We quantitatively characterize the population transfer by FID-detected mmW spectroscopy and observe a population transfer of $\gtrsim$50% in the "counterintuitive" pulse timing, characteristic of STIRAP. In addition, measurement of the population transfer as a function of the Pump and Stokes detunings reveals the characteristic insensitivity of STIRAP transfer to one-photon detunings as long as two-photon resonance is maintained. Numerical simulations of our experiment qualitatively recapitulate these observations.

The optical–mmW STIRAP technique represents a widely applicable method for efficient population transfer into high-ℓ Rydberg states of atoms and molecules. Our simulation of a hypothetical predissociated molecular system demonstrates capability of at least 10% population transfer to a final high-ℓ Rydberg state, despite a 1 ns predissociation lifetime for the intermediate state. All molecules have long-lived high-ℓ Rydberg states, but these states cannot be populated by sequential excitation because optically accessible low-ℓ Rydberg states suffer from fast predissociation. Systematic study of the Rydberg states of many molecules will be made possible by optical–mmW STIRAP, leading to new

applications for molecular Rydberg states in quantum and chemical physics.

Beyond Rydberg states of molecules, the efficient population transfer of the optical–mmW STIRAP technique will be of interest to ultracold experiments on the "trilobite" Rydberg molecules proposed by Greene *et al.*[36] These exotic Rydberg molecules involve a bonding interaction between a ground state atom and an atom in a high-ℓ Rydberg state, which must be excited by a multiphoton scheme. Optical–mmW STIRAP offers an efficient method for accessing the high-ℓ Rydberg manifold and, thus, a productive means for generating the trilobite species. We look forward to exciting implementations of optical–mmW STIRAP in the many areas of Rydberg physics where efficient population of high-ℓ states is desirable.

ACKNOWLEDGMENTS

The authors gratefully acknowledge insightful conversations with Klaas Bergmann (Kaiserslautern) and Stephen Coy (MIT) about this project. The authors thank Trevor Erickson (MIT) for editorial suggestions and Brooks Pate (University of Virginia) for loan of equipment. This material is based on work supported by the National Science Foundation, Award No. CHE-1800410, and the AFOSR, under Award No. FA9550-16-1-0117. D.D.G. was supported by the Department of Defense through the National Defense Science and Engineering Graduate Fellowship Program. T.J.B. was supported by the National Science Foundation Graduate Research Fellowship Program under Grant No. 1122374. J.J. assisted in the preparation of this manuscript at the Lawrence Livermore National Laboratory under the auspices of the U.S. Department of Energy under Contract No. DE-AC52-07NA27344.

DATA AVAILABILITY

The data that support the findings of this study are available from the corresponding author upon reasonable request.

REFERENCES

[1]H. Levine, A. Keesling, A. Omran, H. Bernien, S. Schwartz, A. S. Zibrov, M. Endres, M. Greiner, V. Vuletić, and M. D. Lukin, Phys. Rev. Lett. **121**, 123603 (2018).
[2]S. D. Hogan, C. Seiler, and F. Merkt, Phys. Rev. Lett. **103**, 123001 (2009).
[3]S. D. Hogan and F. Merkt, Phys. Rev. Lett. **100**, 043001 (2008).
[4]F. Merkt and H. Schmutz, J. Chem. Phys. **108**, 10033 (1998).
[5]D. Sprecher, C. Jungen, W. Ubachs, and F. Merkt, Faraday Discuss. **150**, 51 (2011).
[6]D. T. Biernacki, S. D. Colson, and E. E. Eyler, J. Chem. Phys. **89**, 2599 (1988).
[7]E. L. Snow and S. R. Lundeen, Phys. Rev. A **77**, 052501 (2008).
[8]H. Park and R. N. Zare, J. Chem. Phys. **106**, 2239 (1997).
[9]J. Jiang, T. J. Barnum, S. L. Coy, and R. W. Field, J. Chem. Phys. **150**, 154305 (2019).
[10]J. J. Kay, S. N. Altunata, S. L. Coy, and R. W. Field, Mol. Phys. **105**, 1661 (2007).
[11]H. Lefebvre-Brion and R. W. Field, *The Spectra and Dynamics of Diatomic Molecules* (Elsevier, New York, 2004).
[12]T. F. Gallagher, *Rydberg Atoms* (Cambridge University Press, New York, 1994).
[13]J. O. Clevenger, N. A. Harris, R. W. Field, and J. Li, J. Mol. Spectrosc. **193**, 412 (1999).
[14]M. J. J. Vrakking and Y. T. Lee, J. Chem. Phys. **102**, 8818 (1995).
[15]A. Fujii and N. Morita, J. Chem. Phys. **103**, 6029 (1995).
[16]K. Bergmann, H. Theuer, and B. W. Shore, Rev. Mod. Phys. **70**, 1003 (1998).
[17]A. Kuhn, S. Steuerwald, and K. Bergmann, Eur. Phys. J. D **1**, 57 (1998).
[18]T. Halfmann and K. Bergmann, J. Chem. Phys. **104**, 7068 (1996).
[19]K.-K. Ni, S. Ospelkaus, M. H. G. de Miranda, A. Pe'er, B. Neyenhuis, J. J. Zirbel, S. Kotochigova, P. S. Julienne, D. S. Jin, and J. Ye, Science **322**, 231 (2008).
[20]Y. Zhou, "Direct observation of Rydberg–Rydberg transitions via CPmmW spectroscopy," Ph.D. thesis, Massachusetts Institute of Technology, Cambridge, MA, 2014.
[21]Y. Zhou, D. D. Grimes, T. J. Barnum, D. Patterson, S. L. Coy, E. Klein, J. S. Muenter, and R. W. Field, Chem. Phys. Lett. **640**, 124 (2015).
[22]A. L. Steber, B. J. Harris, J. L. Neill, and B. H. Pate, J. Mol. Spectrosc. **280**, 3 (2012).
[23]M. S. Fee, K. Danzmann, and S. Chu, Phys. Rev. A **45**, 4911 (1992).
[24]S. Gangopadhyay, N. Melikechi, and E. E. Eyler, J. Opt. Soc. Am. B **11**, 231 (1994).
[25]A. P. Colombo, Y. Zhou, K. Prozument, S. L. Coy, and R. W. Field, J. Chem. Phys. **138**, 014301 (2013).
[26]U. Gaubatz, P. Rudecki, S. Schiemann, and K. Bergmann, J. Chem. Phys. **92**, 5363 (1990).
[27]D. D. Grimes, T. J. Barnum, Y. Zhou, A. P. Colombo, and R. W. Field, J. Chem. Phys. **147**, 144201 (2017).
[28]C. D. Panda, B. R. O'Leary, A. D. West, J. Baron, P. W. Hess, C. Hoffman, E. Kirilov, C. B. Overstreet, E. P. West, D. DeMille, J. M. Doyle, and G. Gabrielse, Phys. Rev. A **93**, 052110 (2016).
[29]G. Mitchel, B. Grek, F. Martin, H. Pépin, F. Rheault, and H. Baldis, J. Phys. D: Appl. Phys. **11**, L153 (1978).
[30]Z. Kis, A. Karpati, B. W. Shore, and N. V. Vitanov, Phys. Rev. A **70**, 053405 (2004).
[31]M. V. Danileiko, V. I. Romanenko, and L. P. Yatsenko, Opt. Commun. **109**, 462 (1994).
[32]V. I. Romanenko and L. P. Yatsenko, Opt. Commun. **140**, 231 (1997).
[33]N. V. Vitanov, B. W. Shore, L. Yatsenko, K. Böhmer, T. Halfmann, T. Rickes, and K. Bergmann, Opt. Commun. **199**, 117 (2001).
[34]M. Komatsu, T. Ebata, T. Maeyama, and N. Mikami, J. Chem. Phys. **103**, 2420 (1995).
[35]T. Cubel, B. K. Teo, V. S. Malinovsky, J. R. Guest, A. Reinhard, B. Knuffman, P. R. Berman, and G. Raithel, Phys. Rev. A **72**, 023405 (2005).
[36]C. H. Greene, A. S. Dickinson, and H. R. Sadeghpour, Phys. Rev. Lett. **85**, 2458 (2000).